Journal of Structural Geology 34 (2012) 61–76

Contents lists available at SciVerse ScienceDirect

Journal of Structural Geology

journal homepage: www.elsevier.com/locate/jsg

Shear fractures in anisotropic ductile materials: An experimental approach

Enrique Gomez-Rivas [a,b,*], Albert Griera [b]

[a] Department of Geosciences, Eberhard Karls University Tübingen, Wilhelmstr. 56, 72074 Tübingen, Germany
[b] Departament de Geologia, Universitat Autònoma de Barcelona, 08193 Bellaterra, Barcelona, Spain

ARTICLE INFO

Article history:
Received 12 March 2011
Received in revised form
20 October 2011
Accepted 30 October 2011
Available online 9 November 2011

Keywords:
Shear fracture
Anisotropy
Layering
Fracture orientation
Stress field
Multilayer

ABSTRACT

Analogue models have been used to investigate the influence of planar mechanical anisotropy on the orientation of shear fractures in an elastoviscous-brittle material. Multilayered models consisting of a mixture of plasticine, vaseline and preferentially-oriented paper flakes have been coaxially deformed for this purpose. The evolution of the orientation, length and connectivity of fracture sets has been systematically analysed with progressive coaxial deformation. The experimental results show that the orientation of fractures with respect to the deformation axes depends on the orientation of transverse anisotropy. Two symmetrical sets of shear fractures are formed in models with layering parallel to the extension axis *X*, while the fracture network is asymmetrical with respect to the deformation axes for cases with oblique anisotropy. The average dihedral angles between fracture sets are higher than 100°, with the obtuse bisector between the two sets oriented perpendicular to layers. The stress fields calculated from fracture data differ from the boundary conditions applied by the deformation apparatus. This misorientation is related to the degree of anisotropy. In models with high oblique anisotropy both fracture arrays rotate in a dextral sense together with layers towards the *X*-axis, indicating that the presence of a strong anisotropy controls their evolution with progressive deformation.

© 2011 Elsevier Ltd. All rights reserved.

1. Introduction

The mechanical development of brittle fractures and shear bands is a major research topic in the fields of structural geology and rock mechanics (e.g. Scholz, 2002 and references therein). Here, brittle fractures are understood as zones of localised deformation showing strain discontinuities, whereas shear bands are defined as zones of localised deformation with continuous variations of strain across their width. The fundamental controls on the nucleation, propagation and interaction of these structures in isotropic materials are well understood (e.g. Reches and Lockner, 1994; Mandl, 2000; Scholz, 2007). However, many rocks are heterogeneous and anisotropic, and have a different response to normal and shear stress (Cobbold et al., 1971; Platt and Vissers, 1980; Price and Cosgrove, 1990; Weijermars, 1992). It has been previously observed that the presence of a strongly developed planar anisotropy (i.e. compositional layering, foliation, transverse anisotropy, etc.) can affect the nucleation and orientation of fractures and shear bands (e.g. Hanmer et al., 1996; Schöpfer et al., 2006; Welch et al., 2009). For example, Misra et al. (2009) concluded that two shear fracture sets form in systems with a low degree of anisotropy, whereas a high degree of anisotropy enhances the development of only one array. Moreover, the presence of directional heterogeneities enhances the kinematic partition of deformation (Lister and Williams, 1983; Ishii, 1992; Treagus and Sokoutis, 1992; Jiang, 1994; Tikoff and Fossen, 1995; Treagus, 1997, 1998) and can produce a local deviation of the resolved stress field with respect to the regional deformation conditions (Bradshaw and Zoback, 1988; Peacock and Sanderson, 1992).

Most of the classical works analysing the anisotropy influence on fracture orientations were based on experimental data from brittle rocks (e.g. Donath, 1961; Chenevert and Gatlin, 1965; McLamore and Gray, 1967; Hoek, 1968; McGill and Raney, 1970; Attewell and Sandford, 1974; Al-Harthi, 1998). For example, Donath (1961) showed that when transverse anisotropy is oriented either parallel or perpendicular to the maximum principal compressive stress (σ_1), shear fractures develop at an angle ζ of 30°–40° to σ_1 (Fig. 1a), as expected by the Mohr-Coulomb criterion and similar to isotropic rocks (Jaeger and Cook, 1979). This study also showed that shear fractures tend to develop subparallel to anisotropy when the angle between the planar structure and σ_1 varies between 15° and 60°. However, large dispersions of fracture orientations are observed when anisotropy is oriented normal or parallel to σ_1. (e.g. Attewell and Sandford, 1974). In summary, the nucleation of brittle fractures in rocks with transverse anisotropy

* Corresponding author. Department of Geosciences, Eberhard Karls University Tübingen, Wilhelmstr. 56, 72074 Tübingen, Germany. Tel.: +49 7071 29 73147; fax: +49 7071 293060.
E-mail address: enrique.gomez-rivas@uni-tuebingen.de (E. Gomez-Rivas).

0191-8141/$ – see front matter © 2011 Elsevier Ltd. All rights reserved.
doi:10.1016/j.jsg.2011.10.007

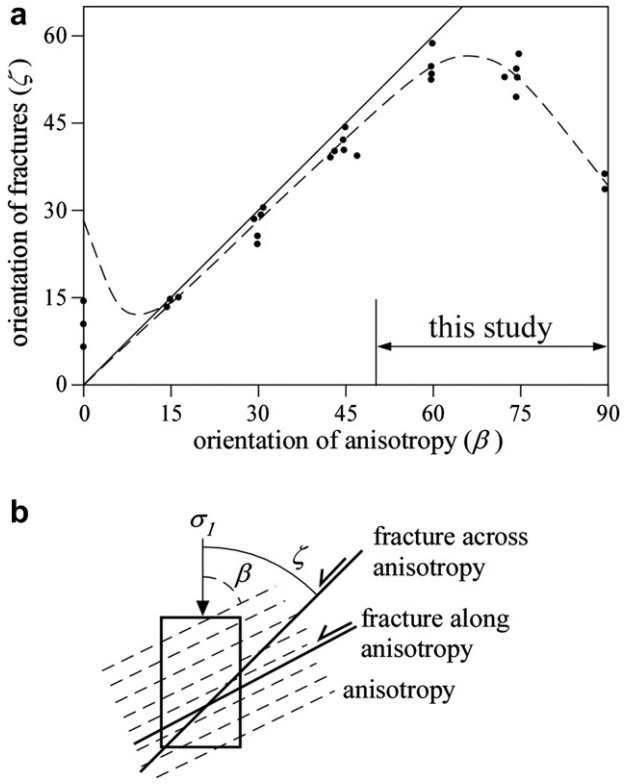

Fig. 1. (a) Graph showing the results from the experiments of Donath (1961) (modified from Twiss and Moores, 1992). When the anisotropy is oriented from 15° to 60° fractures tend to form subparallel to it. Black dots represent data from the experiments of Donath (1961) and the solid line corresponds to fractures parallel to cleavage. The double arrow indicates the orientations analyzed in this study. (b) Definition of the angles between σ_1-anisotropy (β) and σ_1-fracture planes (ζ).

can be described by two failure criteria (Fig. 1b): one along and one across anisotropy, the last one being limited to anisotropy oriented at high angles with regard to σ_1.

However, field observations of anisotropic rocks deformed by dominantly macro-ductile processes (Fig. 2) show that fractures and/or shear bands are not only formed subparallel to anisotropy but also commonly oblique to it (e.g. Platt and Vissers, 1980; White et al., 1980). Some of these structures are interpreted as fractures resulting from the coalescence and linkage of voids (e.g. cracks), in high fluid pressure or local extension conditions. The formation of voids and cavities (e.g. FitzGerald et al., 1991; Stunitz et al., 2003; Vernooij et al., 2006; Arslan et al., 2008; Fusseis et al., 2009; Rybacki et al., 2008) and their collapse and coalescence (e.g. Bons et al., 2004, 2008, 2009) are important precursors of the development of shear bands and shear fractures in mid and lower crust rocks. For example, Fig. 2c shows brittle shear fractures formed from melt pocket collapses in migmatites (Bons et al., 2008).

Experiments of anisotropic materials deformed in a dominant ductile regime (i.e. materials that experience strong viscous deformation before failure) show that, in many cases, the principal direction of shortening bisects the obtuse angle between conjugate shear fractures or shear band sets (e.g. Cobbold et al., 1971; Harris and Cobbold, 1984; Behrmann, 1987; Hanmer et al., 1996; Kidan and Cosgrove, 1996). In such cases, and assuming that σ_1 bisects conjugate sets, the angle ζ between σ_1 and fracture planes is higher than 45°. A value of $\zeta = 45°$ is the predicted orientation by the maximum shear stress or Tresca criterion (Twiss and Moores, 1992; Pollard and Fletcher, 2005). Unusual shear veins at angles higher than 45° in anisotropic rocks have also been described recently by Fagereng et al. (2010). The existence of pre-existing planar fabrics,

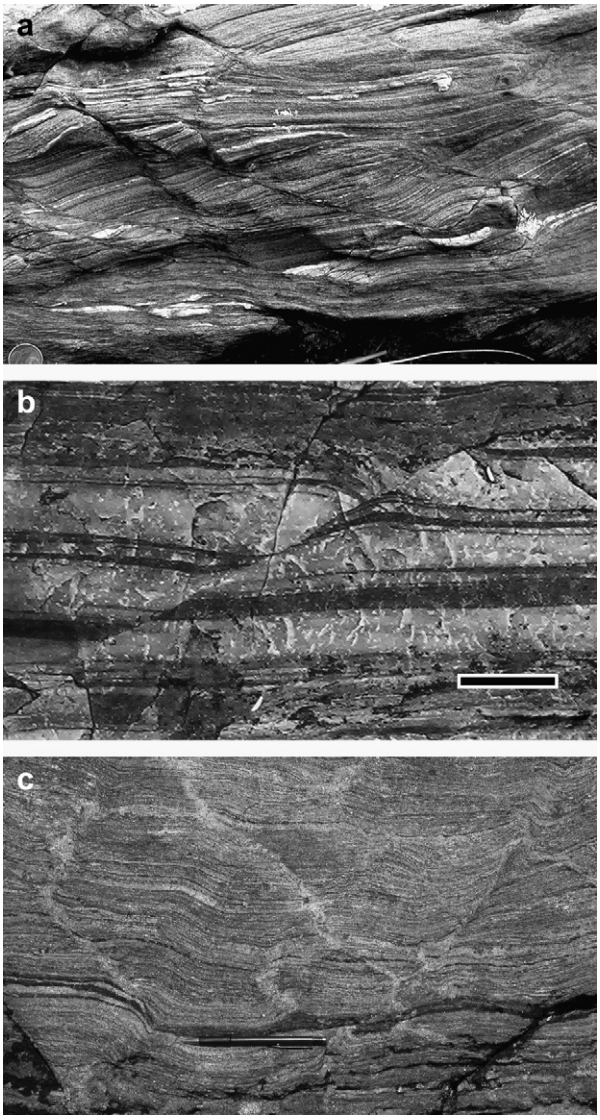

Fig. 2. Examples of brittle fractures oblique to anisotropy in ductile deformed rocks: (a) two sets of fractures in metagreywackes; (b) antithetic isolated small-scale fracture in quartzites (from Gomez-Rivas et al., 2007); (c) conjugate sets of fractures in migmatites, with a symmetric orientation with respect to foliation (courtesy of Paul D. Bons). Photos (a) and (b) are from shear zones from Cap de Creus (E Pyrenees, Spain). Photo (c) is from Port Navalo, France (described in detail by Marchildon and Brown, 2003). The diameter of the 2-cent euro coin is 18.74 mm. The black scale bar is 10 mm long.

high fluid pressures and dissolution-precipitation creep were invoked to explain the active slip along these faults, according to these authors. However, most of the aforementioned works did not systematically analyse the influence of anisotropy orientation on the nucleation and evolution of fractures in an elastoviscous medium.

This paper presents an experimental study of the influence of the orientation of transverse anisotropy on the nucleation and evolution of fractures in an elastoviscous-brittle material deformed under dominant viscous conditions at a constant strain rate. A series of anisotropic plasticine-based multilayers have been deformed coaxially varying the initial orientation of layers with respect to the strain axes imposed by the deformation rig. We aim to analyze how anisotropy influences the orientation, distribution and density of fracture sets with progressive deformation. We focus on situations of deformation at low effective confining pressure

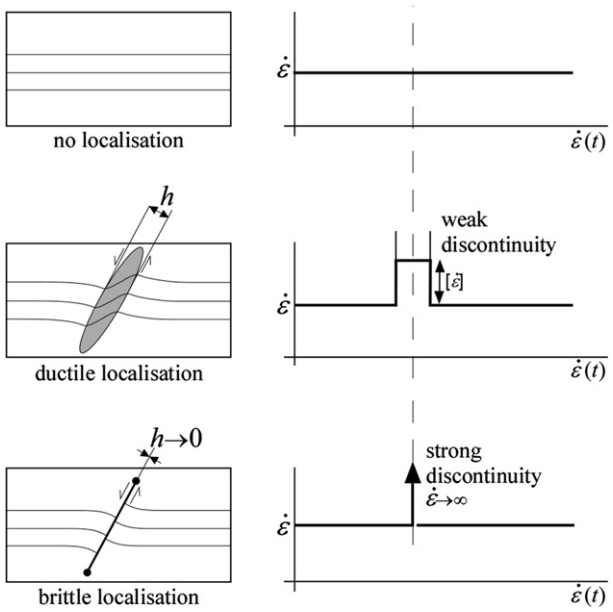

Fig. 3. Sketch illustrating the difference between a shear band (i.e. a structure with a certain band width) and a discrete shear fracture (i.e. an structure that implies a discontinuity surface). Sketch (a) shows a volume of a foliated material subjected to deformation. In this case strain is homogeneously distributed along the material. In (b) a zone of localised deformation with a certain finite width (h) has nucleated. In this case instantaneous deformation is continuous but localised within the band. In (c) a brittle fracture with shear displacement and width $h = 0$ is developed and the instantaneous deformation field is not continuous across the fracture.

conditions, such as middle- to lower crust rocks with high fluid pressures or local extension. It is important to notice that, for simplicity, in this paper we use the term shear fractures for all structures that are discrete planar discontinuities (with loss of cohesion) that produce a shear displacement along them. By definition, a discontinuity resulting from strain localisation has a certain width h (Fig. 3). If the width tends to zero ($h \to 0$), then the displacement field is discontinuous along the surface and the structure is considered a shear fracture (i.e. mode II or III, e.g. Atkinson, 1987). On the contrary, if the localised zone has a certain width ($h \neq 0$) and there is no rupture along the zone (i.e. it is continuous), the structure is considered a shear band. The structures developed in our models are most commonly discrete, but some of them have a certain finite width. To simplify the explanations and analysis both shear fractures and shear bands are treated here as shear fractures. Reference books (e.g. Price and Cosgrove, 1990; Twiss and Moores, 1992; Fossen, 2010) also regard the transition from discrete shear fractures to shear bands as transitional structures without implying a different formation process.

We are particularly interested in analysing and understanding: (1) the influence of anisotropy on the orientation, distribution, density and connectivity of fracture sets; (2) the evolution of the orientation and length of fractures, especially their rotation with progressive deformation; (3) the role of anisotropy on the deviation of the resolved local stress field with respect to the boundary conditions; and (4) the mechanisms controlling the nucleation and propagation of shear fractures in a medium deformed by dominant viscous flow.

2. Materials and methods

2.1. Deformation apparatus

The models were deformed using a strain-rate controlled apparatus that can apply plane strain boundary conditions from pure to simple shear ($0<Wk<1$), at variable temperatures (Fig. 4). This prototype is based on a deformation cell with parallelogram geometry that is originally oriented parallel to a reference frame (X, Z). The cell walls are made of a stack of steel slices that can move between them (Fig. 4a). A computer allows application of a constant strain rate throughout the experiment. Temperature is increased or decreased by a refrigeration circuit that injects either cool or warm oil to an electric fan. Previous experimental studies (Druguet and Carreras, 2006; Bons et al., 2008; Gomez-Rivas and Griera, 2011) were also performed with the same deformation apparatus.

2.2. Analogue materials and their mechanical properties

A mixture of plasticine, vaseline and paper flakes (confetti) was used to simulate the mechanical behaviour of a foliated rock. The models were made by stacking coloured layers (4–5 mm thick) of

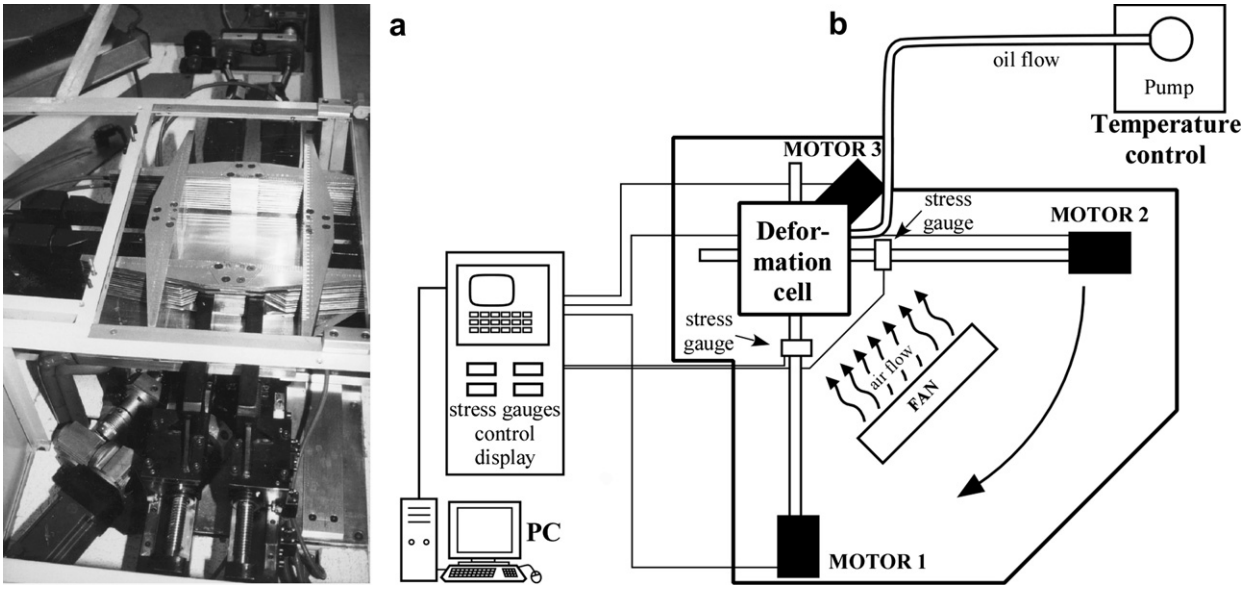

Fig. 4. (a) Photo of the deformation apparatus used in this study and (b) sketch showing the different components of the prototype.

a mixture composed by 80% weight of plasticine (made by the company *Oclu-Plast S.A*, Barcelona), 8 wt. % vaseline and 12 wt. % penny-shaped paper flakes (∅∼2 mm) with a density of 80 gr/m^2. Vaseline was added to decrease viscosity and material strength (Fig. 5) and flakes were inserted to increase anisotropy. Each layer was built with the same amount of plasticine, vaseline and paper flakes. The materials were homogeneously mixed by hand at room temperature and flakes were preferentially oriented parallel to layering using an industrial rolling pin. This procedure also avoided the presence of air bubbles within the models and ensured that flakes were statistically oriented parallel to layers in order to define a transverse anisotropy.

Before carrying out the experiments, the mechanical properties of the analogue materials were characterised using 16 uniaxial compression tests. These tests were made with the same deformation apparatus as the multilayer models, and the same procedure was used to produce them. The methodology we used for that purpose is described with detail in Gomez-Rivas and Griera (2011), and it is based on the studies by McClay (1976), Weijermars and Schmeling (1986), Mancktelow (1988), Ranalli (1995), Schöpfer and Zulauf (2002) and Zulauf and Zulauf (2004).

We tested the rheology of three types of mixtures: (a) white and dark pure plasticine, (b) white plasticine with vaseline and (c) white plasticine with vaseline and paper flakes. Cubes of 10 cm side length of mixtures were deformed at four constant different strain rates: 2×10^{-5}, 6×10^{-5}, 10^{-4} and 2.5×10^{-4} s^{-1} and at a constant temperature of 26 °C up to a minimum shortening of 20%. Additionally, the degree of viscous anisotropy of the material (m) was constrained using two multilayer models with layers oriented at 0° and 40° from the extension direction *X*. These multilayer models were made by stacking 4–5 mm thick layers of anisotropic plasticine mixture.

The results indicate that these mixtures behave as a non-linear elastoviscous material, with a stress exponent which ranges from $n \sim 4$ for the pure plasticine to $n \sim 8$ for the mixture with vaseline and paper flakes (Table 1, Fig. 5). These values were calculated for a reference shortening of 10%, in the same way as Schöpfer and Zulauf (2002). All the stress-strain curves record a strain hardening behaviour throughout the tests (Fig. 5), but only a few of them recorded a clear yield. The value of the effective viscosity ($\eta^* = \sigma/2\dot{\varepsilon}$), of the order of 10^9 Pa s at low strain rates, indicates that our plasticine mixtures are similar to other commercial plasticines used by other authors (Fig. 6, references included in the figure). The degree of anisotropy of these models ($m \sim 6$) was estimated using the analytical method described by Gomez-Rivas and Griera (2009). The model with layers oriented at 0° has a stress peak about 1.4–2.6 times higher than the 40° model. These data also confirm the low difference in anisotropy strength. The addition of dye at the factory makes dark plasticine slightly softer than the white one, although the viscosity contrast between both types of plasticine is very small. On the contrary, the addition of vaseline considerably reduces the material stiffness (see Fig. 5b, Table 1). As we could not run experiments at different confining pressures, we are unable to quantify the resistance of our analogue material to uniform compression (i.e. bulk modulus).

This contribution aims to simulate anisotropic rocks deformed in the middle to lower crust. When the analogue material is deformed, it flows but it can also fracture. It is therefore suitable for simulating a rock that exhibits elastoviscous and brittle behaviour.

Table 1
Parameters calculated from the compression tests to characterize the mechanical properties of the analogue materials. All these values were calculated at a shortening of 10%.

Composition	Axial stress (σ) [Pa]	Effective viscosity (η) [Pa s]	Stress exponent (n)	Material constant (C) [Pa^{-n} s^{-1}]
White pure plasticine	$2.5 \cdot 10^4$	$6.2 \cdot 10^8$	3.9	$1.8 \cdot 10^{-22}$
Dark pure plasticine	$2.4 \cdot 10^4$	$6.0 \cdot 10^8$	4.1	$3.5 \cdot 10^{-23}$
White plasticine + vaseline	$1.1 \cdot 10^4$	$2.8 \cdot 10^8$	6.9	$4.3 \cdot 10^{-33}$
White plasticine + vaseline + paper flakes	$2.9 \cdot 10^4$	$7.3 \cdot 10^8$	8.1	$2.1 \cdot 10^{-40}$

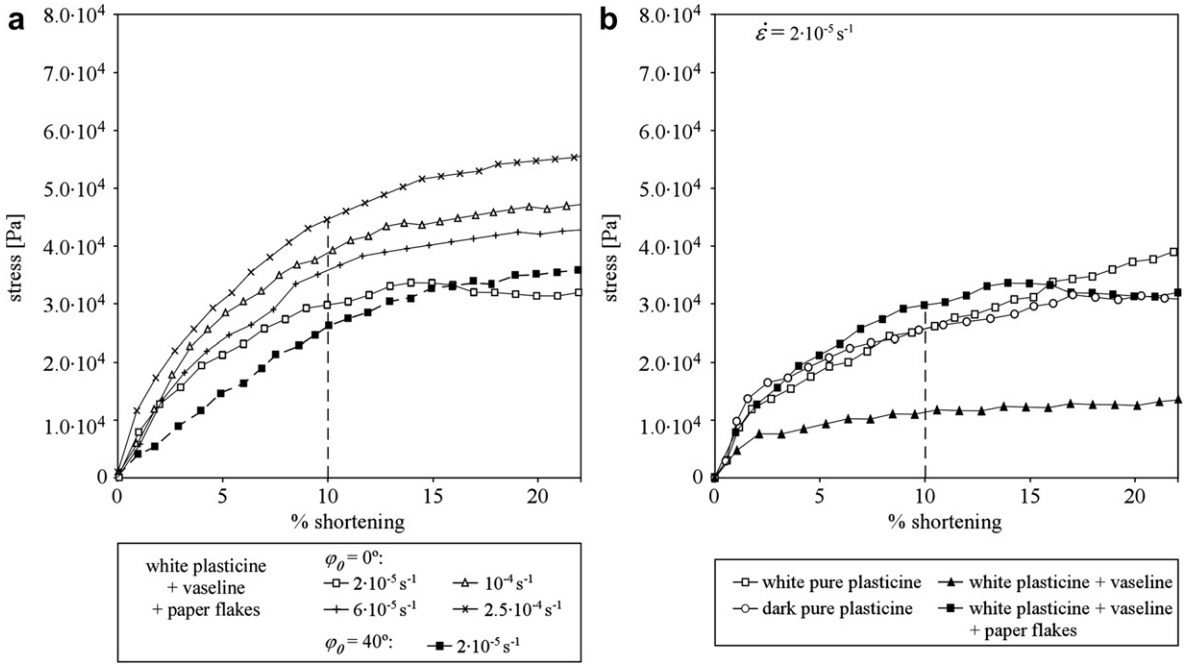

Fig. 5. Strain-stress curves of different experiments: (a) graph of models made of white plasticine with vaseline and paper flakes deformed at different strain rates (initial orientation of layers with respect to *X*: $\varphi_0 = 0°$ and 40°); (b) curves of four different mixtures deformed at the same strain rate ($\dot{\varepsilon} = 2 \cdot 10^{-5}$ s^{-1}). Dashed lines indicate the strain reference value for comparing the properties of the materials.

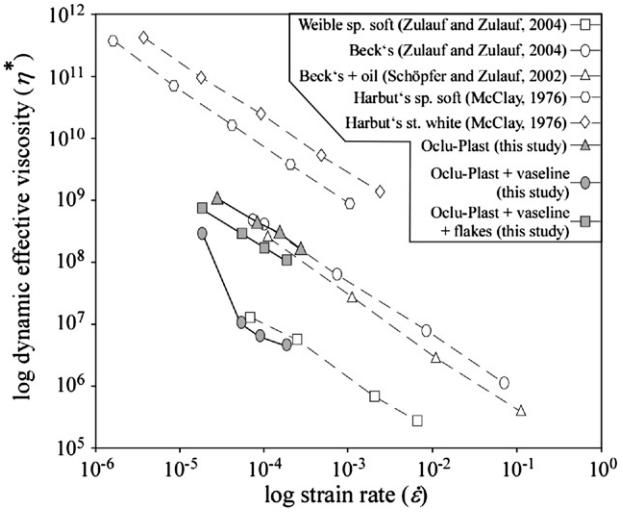

Fig. 6. Log diagram of strain rate *vs*. effective dynamic viscosity comparing the plasticine used in this study with other commercially available plasticines analysed by other authors. All the values of effective dynamic viscosity were taken at a shortening of 10%. The data from our material is an average of purple and white plasticine.

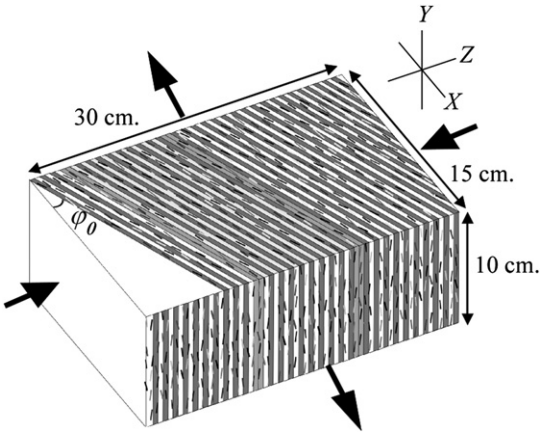

Fig. 7. Sketch of a multilayer model: φ_0 is the initial angle of the layering with regard to the extensional axis *X*. Arrows show the direction of σ_1 applied by the deformation apparatus.

The mechanical and time scaling between the analogue material and simulated natural rocks (Pfiffner and Ramsay, 1982; Davidson et al., 1994) are summarized in Table 2. Assuming a natural strain rate value of 10^{-14} s^{-1}, one experimental second is equivalent to approximately 60 natural years, making the viscosity of the analogue material equivalent to the inferred viscosity of lower crust rocks (10^{19} Pa s, Davidson et al., 1994), and of the same order of the ones used in other studies (Zhang et al., 1996; Mancktelow, 1999). A geometrical scaling of 1:1 is assumed for our models.

2.3. Model set-up and deformation conditions

The multilayer models were made up of alternating 4–5 mm thick layers of differently coloured anisotropic plasticine mixture, oriented at an initial angle φ_0 to the *X* extension direction (Fig. 7). This angle ranged from 0° to 40° at increments of 10°, giving a total of five experiments. The models were deformed under coaxial conditions at a constant strain rate of $2\cdot10^{-5}$ s^{-1} and a temperature of 26 °C. All the samples were deformed until 50% shortening. During deformation, the models were compressed in the *Z* direction and extended in the *X* direction (unconfined, $\sigma_3 \sim 0$), while the *Y* direction was constrained using a reinforced transparent glass. The initial size of the models was 30 × 15 × 10 cm (Fig. 7). White and dark layers were stacked alternatively, and two layers made of a combination of both mixtures (grey coloured) were inserted at 10 cm from the top and bottom of the models (perpendicular to *Z*) to facilitate the identification of layers at different stages of deformation. Before starting deformation, each model was hydrostatically compressed for 24 h at approximately 10 kPa in order to stick layers together to avoid interlayer slipping and hence make cohesive models.

Before carrying out the final series of experiments, which contain paper flakes and oblique layering, we developed multilayer models with different combinations of plasticine, vaseline and flakes to study the effects of progressively adding components to pure plasticine. These experiments were used to define a reference frame in order to understand the development of structures in each case (Fig. 8) and to test the effects of variable anisotropy on in the deformation processes and microstructures.

Temperature and strain rate were automatically controlled and the evolution of the stress (σ) was recorded using four gauges parallel to the extension and compression axes, with a precision of ~0.15 kPa (see Fig. 4b). Digital pictures of the upper surface were taken every 1% of shortening. Vaseline was used to lubricate the interfaces between the models and the press boundaries to minimize friction. Glycerine was used instead at the contact of the top surface of the model to allow a clear view of the top of the sample.

A constant area of 100 cm^2 at the centre of each model was selected for the sampling of data and their subsequent analysis (Fig. 8d). This sampling method aimed to avoid boundary effects (e.g. friction). A sketch of the fracture network was drawn at intervals of 10% of shortening. The main parameters measured were the fracture length, their connectivity and the angle (δ) of the shear fractures/bands with regard to *Z*. The evolution of these parameters was measured for every fracture developed within the sampling area. All these data were collected from digital pictures of the upper surface at constant shortening intervals. The use of paper flakes and layers of different colours allowed us to use them as markers to track deformation. Additionally, a particle image velocimetry (PIV) code (Bons and Jessell, 1995) was used to test the robustness and validity of our fracture measurements.

Table 2
Values of strain rate and effective viscosity of mid crustal rocks and the analogue materials used in this study. The strain rate value for mid crustal rocks is from Pfiffner and Ramsay (1982) and Weijermars (1997). The estimated range of viscosities of schists is from Davidson et al. (1994).

Material	Strain rate ($\dot{\varepsilon}$)	Deformation time (50% sh.)	Effectiv viscosity (η^*)
Mid crustal rocks (schist at 500–700 °C)	10^{-14} s^{-1}	$8.25\cdot10^{13}$ s (~2.6 Myr)	$\sim10^{18}$–10^{19} Pa s
Experimental mixture (plasticine + vaseline + flakes)	$2\cdot10^{-5}$ s^{-1}	$3.5\cdot10^{4}$ s	$\sim10^{9}$ Pa s

3. Experimental results

3.1. Analogue materials

With the objective of establishing a reference framework of our multilayer experiments, Fig. 8 shows a visual comparison of the influence of the four different analogue materials used in this study on the development of structures and the style of deformation: (A) pure plasticine, (B) plasticine mixed with 9% vaseline, (C) plasticine

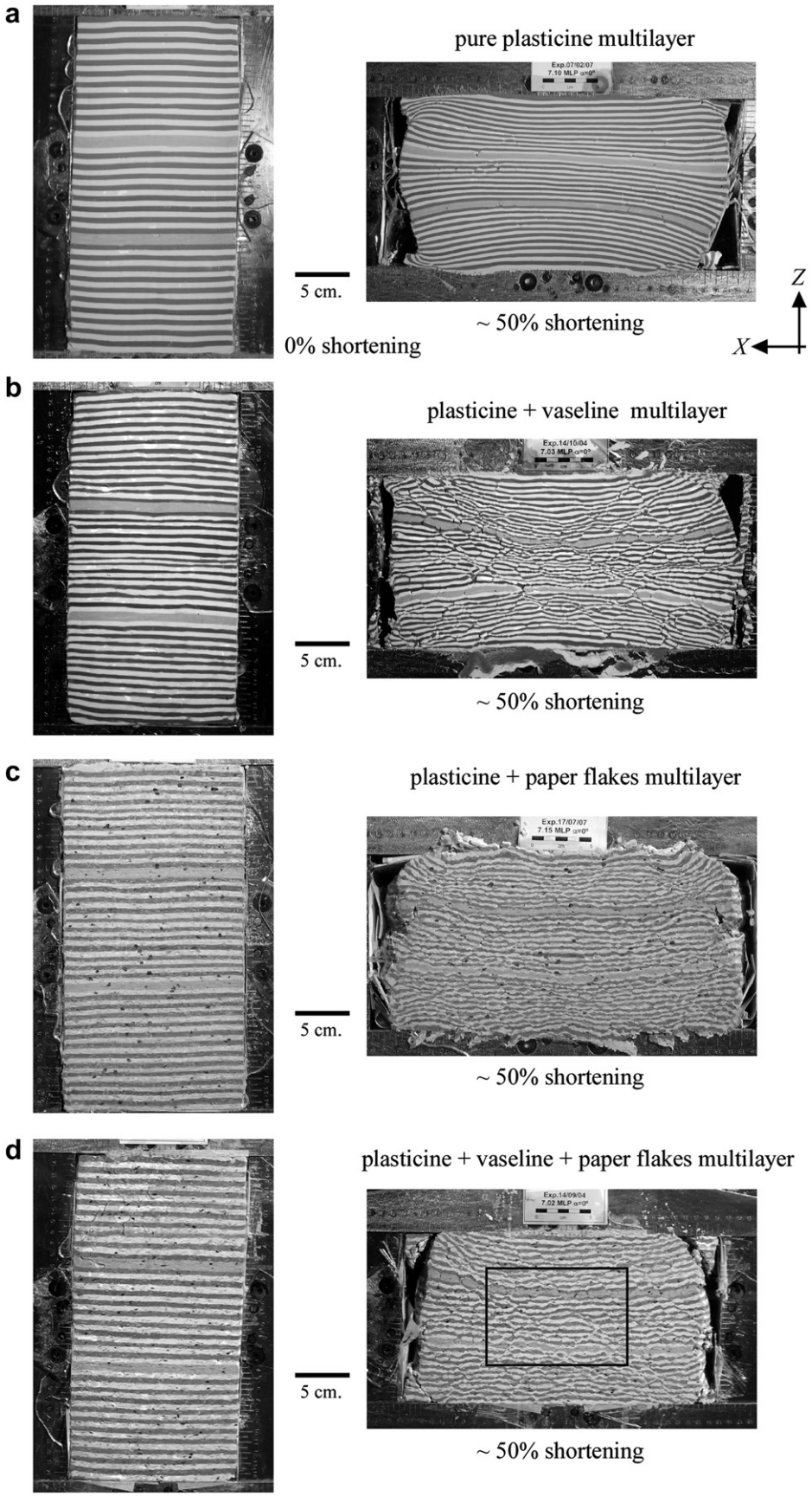

Fig. 8. Initial and final state of different experiments used to make a reference frame for our series of models: (a) multilayer model made of layers of pure white and dark plasticine; (b) multilayer model of white and dark plasticine layers mixed with 8% wt. of vaseline; (c) multilayer model made of white and dark layers of plasticine mixed with 12% wt. paper flakes; (d) multilayer model of white and dark layers of plasticine mixed with 8 wt. of vaseline and 12% of paper flakes. The black rectangle shows the sampling area where data was collected. We finally used the composition of model (d) for our main series of experiments.

mixed with 12% paper flakes and (D) plasticine mixed with 9% vaseline and 12% paper flakes.

3.1.1. Pure plasticine

The model made with pure plasticine (model A) was deformed by viscous flow and almost no fracturing could be observed, except for a small number of tension cracks (Fig. 8a). In this case, layers were thinned with progressive deformation and the cracks only developed after >40% shortening. While the central part of the models was essentially homogenously deformed, the four corners behaved heterogeneously due to boundary effects (Fig. 8a). Interlayer slipping or traction structures along layer interfaces were not observed.

3.1.2. Plasticine plus vaseline

The behaviour of pure plasticine is strongly modified when vaseline is added to it (model B) (Fig. 8b). In this case strain was localised in a large number of tension cracks that later on led to the development of a complex network of shear fractures. Fig. 9a–b shows intermediate stages (20% and 30% shortening) of the evolution of structures in the central region of this model. The first fractures were straight tension cracks that quickly propagated perpendicularly to layering. These cracks developed into open voids, with lengths that reached 2–3 times the layer thickness. With progressive deformation these cracks interacted to cause a rapid coalescence and collapse of voids, giving rise to many large conjugate shear fractures. These results indicate that the addition of vaseline causes the development of tension cracks and voids by cohesion reduction, and enhances fracture nucleation.

3.1.3. Plasticine plus paper flakes

The insertion of paper flakes preferentially oriented parallel to layering (model C) also enhances fracture development (Fig. 8c). However, there are important differences in the style of deformation between this mixture and the previous model. When paper flakes are present, large tension cracks are not observed and a large number of millimetre-scale voids formed at the interfaces between layers or between flakes and plasticine (Fig. 9c–d). The geometries of these voids are irregular, including many with zigzag and dimpled patterns. The presence of flakes, which are stiffer than plasticine, causes strain localisation at their tips. They also inhibit the propagation of large tension cracks, because they cannot propagate through flakes. In the models B and C some shear fractures and shear bands nucleated from voids and lead to the development of two conjugate fracture sets (Fig. 8b and c). Additionally, the amplification of layer thickness irregularities led to the development of pinch-and-swell geometries that progressively evolved to form shear fractures. They were generally oriented at high angles with regard to the *Z*-direction.

3.1.4. Plasticine plus vaseline and paper flakes

A similar behaviour was observed in the model D, made of a mixture of plasticine, vaseline and paper flakes (Fig. 8d), which was the composition used to make the final series of experiments (i.e. with different initial orientations of layers with respect to the deformation axes). In this case large tension cracks could not nucleate and two sets of shear fractures were formed. Details of the type of structures and the geometry and orientation of shear fractures will be described in the following sections. The advantage of

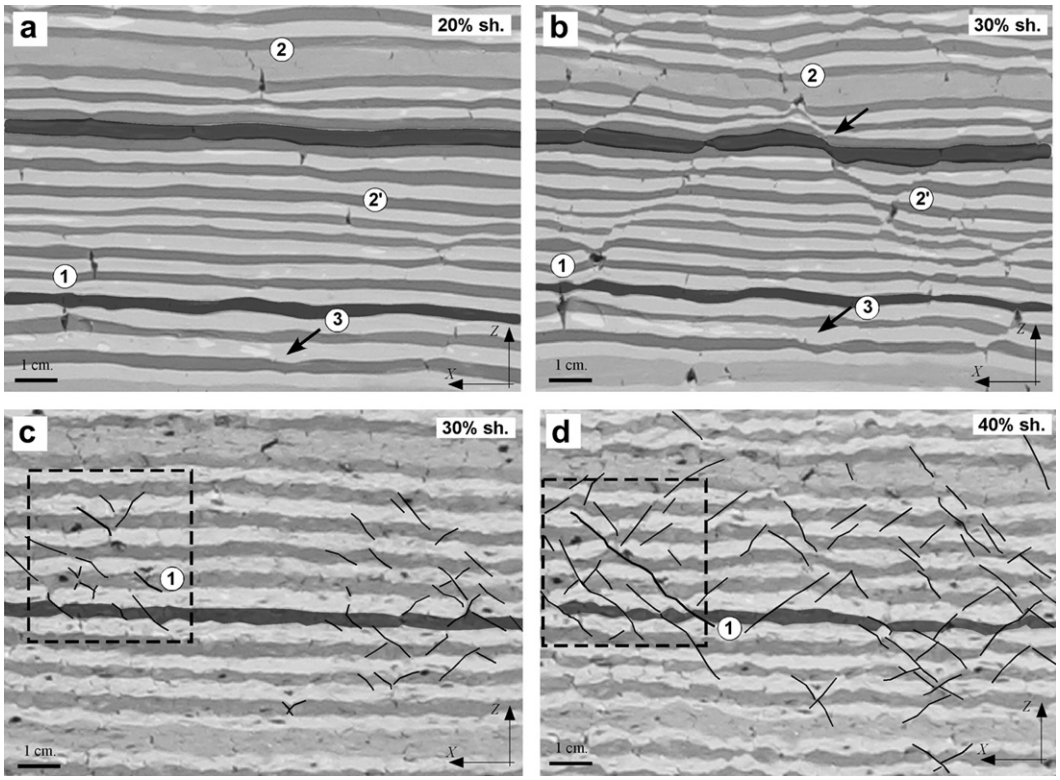

Fig. 9. Detailed photographs of a $\varphi_0 = 0^\circ$ model made of plasticine and vaseline (a–b) and a $\varphi_0 = 0^\circ$ model with paper flakes (c–d). (a–b): (1) Propagation of a tension crack and nucleation of shear fractures from crack collapse; (2–2′) Interaction between open cracks that lead to the formation of a shear band; (3) Heterogeneous thinning of layers that lead to the formation pinch-and-swells and later nucleation of shear bands. (c–d): layers and paper flakes are used as markers to follow flow and displacement along fractures. These markers indicate that interlayer slip is low. In models with paper flakes (c–d) tension crack propagation is considerably lower than in models without flakes. Progressive analysis of digital images of the experiments allows us to track the growth and coalescence of shear fracture networks, (solid black lines). (1) Coalescence of fracture segments causes variable displacements along large fractures. Dark grey layers have been painted in this figure as visual references. The black dashed box indicates a detailed area where all observed faults have been drawn.

using this mixture (i.e. plasticine, vaseline and flakes) is that vaseline facilitates sample preparation and allows the insertion of paper flakes, because it increases the ductility of plasticine. Also, the presence of paper flakes increases the degree of anisotropy and the adhesion between layers. Paper flakes also serve as markers and help us following the evolution of structures. The tracking of displacements between layers using paper flakes does not show a slip component parallel to anisotropy (see Fig. 9c and d). These observations are also valid for models with anisotropy initially oriented oblique to the *X*-direction.

3.2. Nucleation of structures

During the first stage of the experiments deformation was accommodated mainly by homogeneous flow and, for the experiments with oblique anisotropy ($\varphi_0 > 0^\circ$), layer rotation towards the *X*-direction (Fig. 10). During this stage, stress increased up to reach the yield stress at 15%–18% of shortening, which occurred approximately with the nucleation of the first visible macroscopic structures (pinch-and-swell, boudinage, tension cracks and some shear fractures). All the models registered slight strain hardening after yielding.

Pinch-and-swell and boudinage developed due to (a) the slight competence contrast between plasticine layers (i.e. white layers are slightly more viscous than dark ones) and (b) mainly by the presence of paper flakes. Symmetric and asymmetric boudinage are formed due to the interaction of tension cracks or because of flow discontinuities next to paper flakes. Development of conjugate sets of shear fractures arose from void or tensional crack collapse, progressive necking of pinch-and-swell structures or direct nucleation unrelated with previous structures (Fig. 10).

The propagation and coalescence of fractures led to the development of lozenge shaped zones where deformation was considerably lower and evenly distributed. Volume loss by compaction was estimated about 6% after 50% of shortening. This loss is shown by the opening of free space in the extensional direction between the models and the deformation apparatus (Fig. 8). The analysis of intermediate deformation stages allowed us to accurately track the evolution of fracture-segment coalescence that lead to the formation of larger fractures. Using layers and paper flakes as reference

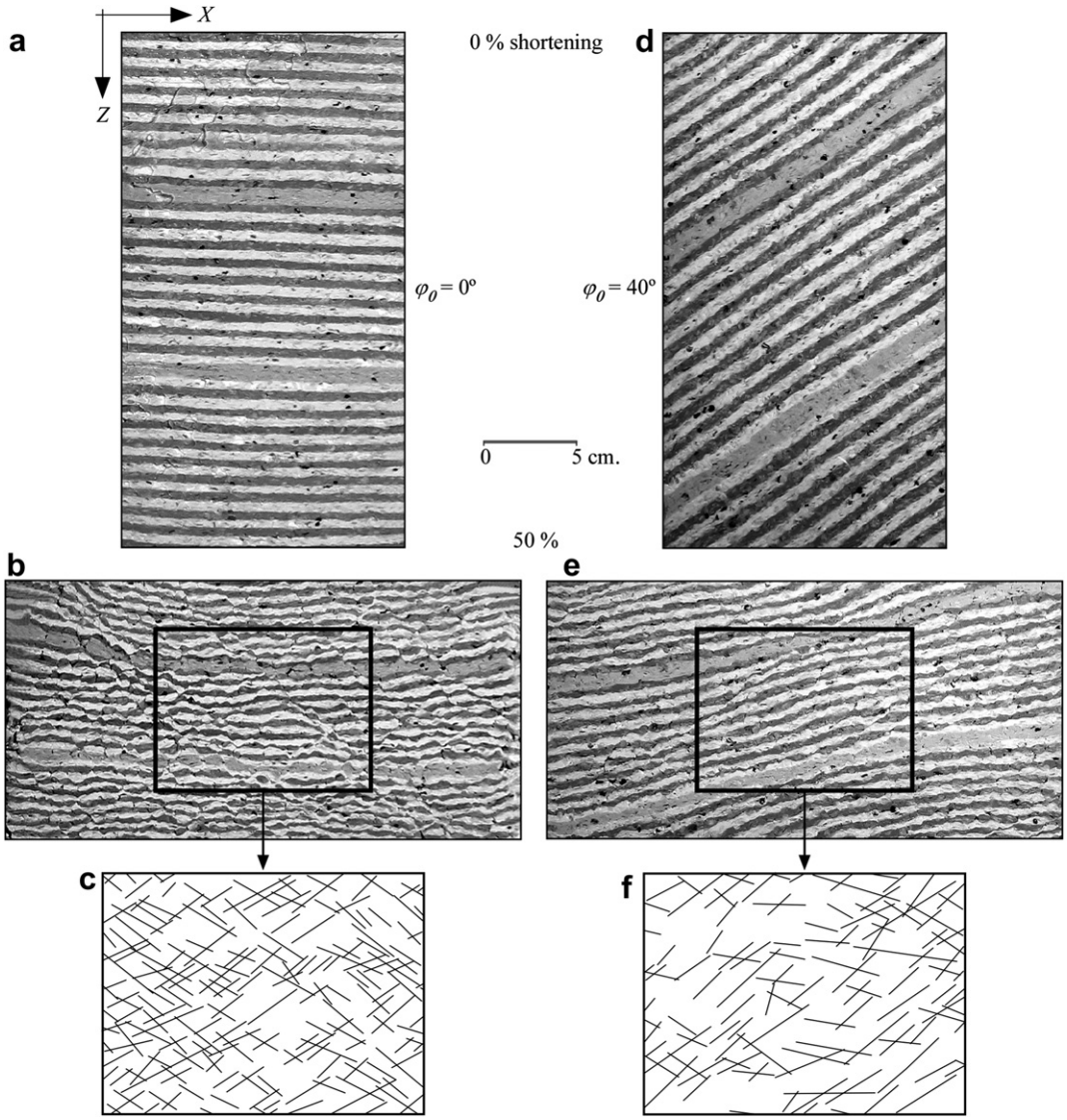

Fig. 10. Photographs of the initial and final stages of the experiments with layering parallel to the extension axis (a–b, $\varphi_0 = 0^\circ$) and oblique to it (d–e, $\varphi_0 = 40^\circ$). The final stage corresponds to 50% of shortening in both experiments. The black rectangle shows the sampling area where data were collected. (c) and (f) are sketches of all the fractures that could be identified and analysed.

markers, the displacement along fractures can be measured. The values of accumulated displacements along fractures are variable, with zones of maximum and minimum displacement (see fracture (1) in Fig. 9c) and illustrate the complexity of the shear fracture network formed by coalescence.

3.3. Shear fracture geometry and orientations

Maps of finite strain ratio (*Rf*) at deformation intervals of 10% shortening were compared with interpreted fracture maps (Fig. 11). Regions of high strain associated with shear fractures are developed across layers. These zones are oriented at relatively high angles (~45°–55°) with respect to the layer normal. They are consistent with the measured conjugate shear fractures. Lower-strain lozenge zones are also distinguished. These observations confirm that our measurements are consistent and allowed us to manually draw and measure sketches of fractures, avoiding the lower resolution of PIV measurements.

In our experiments, fractures were mostly planar and normal to the simple top surface (i.e. parallel to the *Y*-axis). Therefore, they were characterized in 2D as traces on the X-Z plane. Fracture sets of the different experiments have average lengths ranging between 1.3 and 2.0 cm, with standard deviations between 0.34 and 0.77. No systematic refraction of fractures has been observed across layers, supporting the inferred low viscosity contrast between dark and white plasticine layers. A low degree of connectivity between fractures is observed, with values ranging between 10% and 35% at the final stage of the experiments (Table 3). This means that most of the fractures remained isolated throughout the experiment. Fractures of the set with a sinistral shear sense have a higher connectivity than the dextral set, especially in oblique models (i.e. $\varphi_0 > 0°$).

Two conjugate sets of shear fractures were formed in the models with layers parallel to *X* ($\varphi_0 = 0°$) (Fig. 12). Structures of both sets (dextral and sinistral) started to be visible at a shortening of 15–20% with an average angle $\delta = 55°–58°$ with regard to *Z*. However, the variability in angles is quite large, with individual values ranging between 39° and 67° and a standard deviation of 7°. In contrast to $\varphi_0 = 0°$, the models with oblique anisotropy ($\varphi_0 > 0°$) show an asymmetrical pattern of the orientation of fracture sets with respect to *Z*. In this case, the dextral set nucleated at a higher angle to the *Z* axis than the sinistral one, which tended to be oblique to the layering. With progressive deformation, layering rotated towards the *X* direction and shear fractures nucleated during the last stages of the experiments tended to be arranged more symmetrically. There is a clear relationship between the initial obliquity of anisotropy (φ_0) and the density of shear fractures developed for each case (Table 4, Fig. 12).

Table 3
Fracture connectivity, measured as the percentage of fractures that are connected to others at 50% of shortening.

φ_0	Sinistral set	Dextral set
0°	23%	20%
10°	37%	17%
20°	35%	12%
30°	31%	18%
40°	8%	15%

In order to quantify the degree of fracturing, a fracture index (*FI*) has been defined as the number of fractures per unit length, using a line-intercept method by taking a sample direction perpendicular to the average orientation of each fracture set (Hudson and Harrison, 1997). The results of the *FI* analysis, presented in Fig. 13, quantitatively corroborate the observation that the sinistral set, which has a shear sense opposite to the rotation of anisotropy and intersects the layers at an acute angle, is the dominant array in the experiments with $\varphi_0 > 0°$. Furthermore, the increase of the initial obliquity of layering reduces the development of fractures. For instance, the *FI* of the dextral set in the $\varphi_0 = 0°$ model is almost double than that of the same set in the $\varphi_0 = 40°$ experiment. From two dimensional studies, and at least for coaxial conditions, the ratio between the *FI* of the two sets of fractures is a potential indicator of the obliquity of layering with respect to the maximum compression axis. However, this ratio tends towards a value of 1 at high strain as the anisotropy rotates towards the *X*-direction.

Fig. 14 and Table 5 show the mean nucleation orientation of new macroscopic fractures (i.e. the orientation of the first time a fracture was visible) and their evolution with progressive deformation. The data were sampled using regular intervals of 10% of shortening, and the mean values calculated for each set. For $\varphi_0 = 0°$ experiments, the two sets of shear fractures rotated towards the extension direction *X*, but at a lower angular velocity (ω) than the one expected for a passive material line. In models with oblique layers ($\varphi_0 > 0°$), the sinistral set of fractures rotated towards the extension direction while the dextral set moved away from the extension direction and rotated in a clockwise sense together with layering, but with an angular velocity slower than layers.

The average dihedral angles between both fracture sets range from 100° to 120° and are uniform in all the models (Tables 4 and

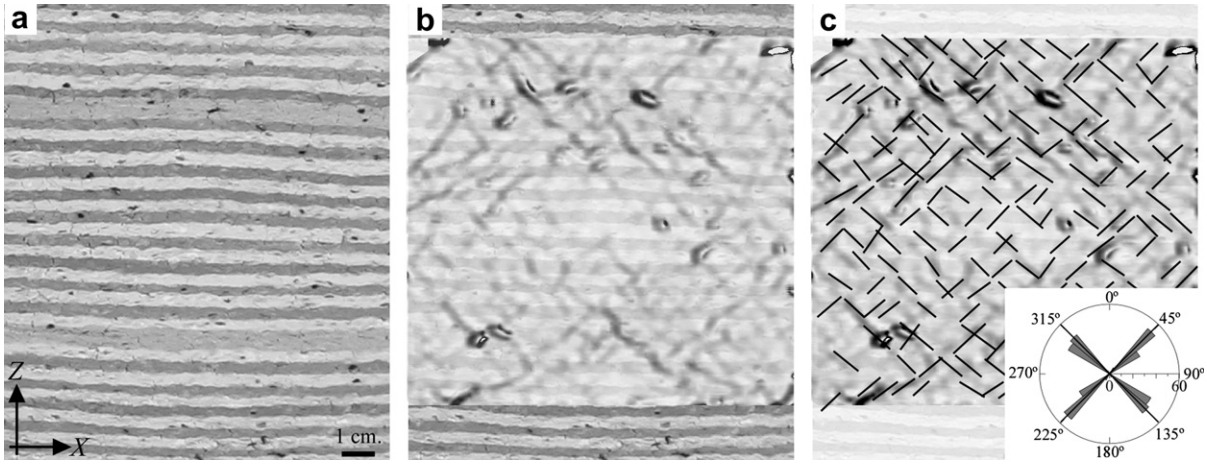

Fig. 11. Comparison of a finite strain ration (*Rf*) map made using a PIV method (b) and the hand-draw sketch of the fracture network (c) based on digital pictures of the $\varphi_0 = 0°$ experiment (a). The coincidence of both analyses corroborates the validity of our fracture network orientation measurements.

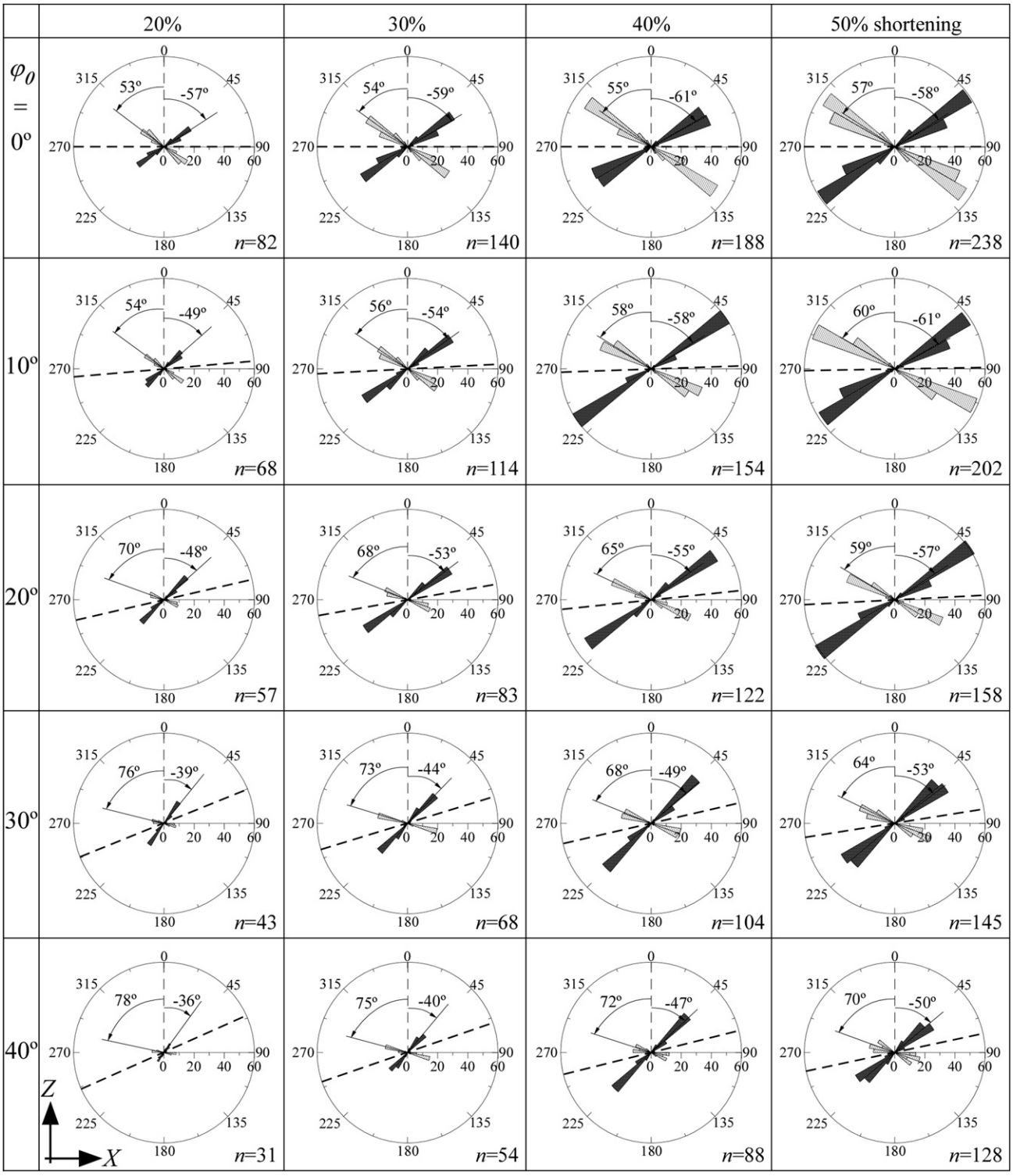

Fig. 12. Rose diagrams of the orientation (δ) and the population of fractures (at orientation intervals of 10°) of all the studied experiments. The average orientation of each fracture set with respect to the *Z* axis is indicated. Dark grey clusters correspond to the sinistral set of fractures, while light grey clusters represent the data of the dextral set. Dashed lines indicate the orientation of anisotropy. *n* is the number of data measurements in each diagram.

5). Following the observations from the $\varphi_0 = 0°$ model, the angles at which new fractures nucleated did not substantially change with progressive deformation and new fractures were formed with orientations similar to the earlier ones.

The rate at which fractures propagated can be estimated using the variation of the length during a constant interval of shortening or time. The propagation rate of the fracture ensemble ($\dot{l}$) has been defined as:

$$\dot{l} = \frac{1}{l}\frac{\mathrm{d}l}{\mathrm{d}t} \tag{1}$$

Table 4
Compilation of the average orientations of fractures sets (δ) at shortening intervals of 20, 30, 40 and 50%. The number of data measurements (n) and the mean standard deviation (σ) are also listed.

φ_0		Sinistral set of fractures				Dextral set of fractures			
		20%	30%	40%	50% sh	20%	30%	40%	50% sh.
0° New fractures	20% sh.	−57°	−59°	−62°	−58°	53°	56°	57°	58°
	30%		−58°	−61°	−60°		51°	55°	59°
	40%			−59°	−59°			52°	61°
	50%				−53°				56°
	Mean	−57°	−59°	−61°	−58°	53°	56°	56°	57°
10°	20%	−49°	−54°	−57°	−60°	54°	56°	58°	61°
	30%		−54°	−60°	−63°		55°	59°	60°
	40%			−58°	−62°			57°	61°
	50%				−60°				56°
	Mean	−49°	−54°	−58°	−61°	54°	56°	58°	60°
20°	20%	−48°	−53°	−56°	−58°	70°	67°	64°	59°
	30%		−52°	−55°	−61°		69°	66°	62°
	40%			−54°	−58°			65°	57°
	50%				−58°				52°
	Mean	−48°	−53°	−55°	−59°	70°	68°	65°	57°
30°	20%	−39°	−44°	−48°	−53°	76°	74°	70°	66°
	30%		−44°	−48°	−54°		70°	67°	64°
	40%			−50°	−52°			67°	64°
	50%				−51°				62°
	Mean	−39°	−44°	−49°	−53°	76°	73°	68°	64°
40°	20%	−36°	−40°	−48°	−50°	78°	76°	72°	70°
	30%		−41°	−45°	−49°		75°	73°	69°
	40%			−48°	−52°			70°	67°
	50%				−48°				72°
	Mean	−36°	−40°	−47°	−50°	78°	75°	72°	70°

where l is the average fracture length and t is time. After the initial nucleation stage (at 20% shortening) the rate $\dot{l}$ ranged between $2\cdot10^{-4}$ and $2\cdot10^{-5}$ s^{-1}. These values are of the same order or one order of magnitude higher than the bulk strain rate of the experiments. The propagation of fractures depends on the obliquity of anisotropy. The maximum propagation values correspond to the $\varphi_0 = 0°$ experiment, while a decrease in the propagation rate of fractures was observed with increasing the obliquity of anisotropy with the X-axis. At a high strain these values were similar in all experiments. This observation seems coherent if we take into account that the material and the strain rate were the same in all the experiments. Therefore, the rotation of layering during the initial deformation stages in oblique experiments reduced both the development of fractures and their propagation rate.

4. Discussion and interpretation of the experimental results

The experimental results presented in this contribution demonstrate that the orientation of anisotropy has a strong influence on the orientation of shear fractures in elastoviscous-brittle materials. It controls the transition from systems in which two symmetrical sets of fractures develop to experiments with an asymmetrical arrangement of fractures. These results contribute to the understanding of controls on fracture orientations in ductile materials (i.e. materials deformed without loss of cohesion at the bulk scale or without discontinuity in the displacement field; e.g. Twiss and Moores, 1992), as well as to the evolution of such fracture networks with progressive deformation.

4.1. On the influence of anisotropy on the nucleation angle of shear fractures

The angle at which shear fractures nucleate and propagate is a key parameter in understanding how the material behaves when it is subjected to deformation. The experimental results show that the orientation of new shear fractures depends on the relative orientation of anisotropy and stress field geometry (Fig. 14).

Using classical failure criteria (see Twiss and Moores, 1992; Pollard and Fletcher, 2005), we find that an expression of the angle at which shear fractures nucleate (δ) with respect to the Z-axis can be described as:

$$\delta \sim f(\phi, \psi, \varphi) \tag{2}$$

where ϕ is the angle of friction, ψ is the dilatancy angle (Vardoulakis, 1980) and φ is the angle between anisotropy and the reference system. Due to the plastic and low frictional behaviour of plasticine, and the lack of experimental data at different confining pressures, we have assumed an ideal plastic non-frictional behaviour and, consequently, a value of the internal friction angle of $\phi = 0°$ (McClay, 1976; Zulauf and Zulauf, 2004). The dilatancy angle can be constrained using the experiment with $\varphi_0 = 0°$ assuming that it corresponds to the deviation angle between the measured fracture orientations and the ones predicted by the Mohr-Coulomb criterion (i.e. δ=45°). Using this approach we have estimated a dilatancy angle of $\psi = -20°$. A dilatancy angle of 0° would correspond to an incompressible material (Poliakov et al., 1994), while a positive value is related to a dilatation of the material during failure. Therefore, negative

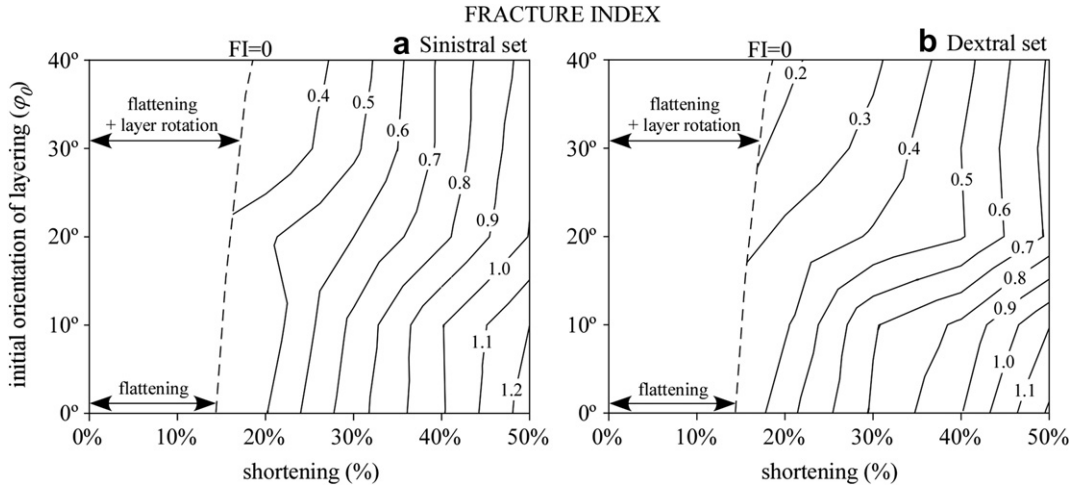

Fig. 13. Contour plots of the fracture index (FI), expressed in cm^{-1}, for all the analysed models: (a) sinistral set and (b) dextral set.

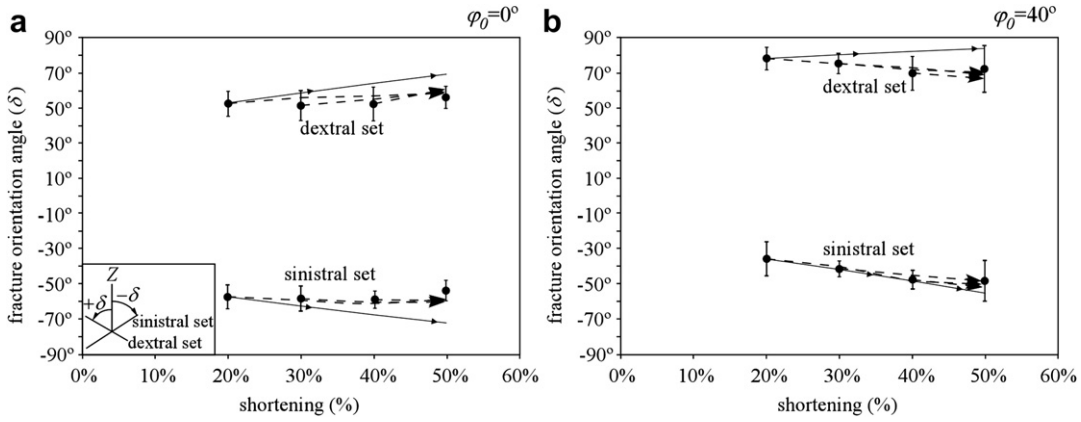

Fig. 14. Mean orientation of new shear fractures (filled circles) and their evolution with progressive deformation (dashed lines) for (a) $\varphi_0 = 0^\circ$ and (b) $\varphi_0 = 40^\circ$ models. Fracture orientations δ are indicated with respect to the shortening axis (Z). These values have been measured at intervals of 10% of shortening. Solid curves show the theoretical evolution of a passive marker oriented similar than fractures at 20% of shortening. The error bars represent the standard deviation values of each data set.

values of the dilatancy angle can be interpreted as a sign of compactional behaviour of the material. During the experiments, the plasticine mixture is progressively compacted, as evidenced by a total volume loss of about 6% after 50% shortening. Taking into account these observations and the results from the experiments with general anisotropy orientations, the equation (2) can be expressed as a linear dependency:

$$\delta = \pm 45^\circ \mp \frac{\psi}{2} + \frac{\varphi(\varepsilon)}{2} \tag{3}$$

where δ is measured counter clockwise with regard to Z and $\varphi(\varepsilon)$ accounts for the orientation of layering with progressive deformation. For our experiments, $\delta > 0^\circ$ values correspond to the dextral set while $\delta < 0^\circ$ values is used to describe the sinistral array of fractures. Therefore, equation (3) is not only restricted to low strain and it is able to predict the finite orientation of shear fractures in all our models throughout time with an adequate precision (Fig. 15, Table 5).

Table 5
Average orientation of the new fractures identified at 20, 30, 40 and 50% shortening and their evolution with increasing deformation. The population of data has been divided according to their nucleation interval and subsequent rotation with the increase of the deformation. The number of data used for each interval is presented in Table 4. φ_0 is the initial orientation of layering with the maximum stretching axis X.

φ_0	% sh.	Sinistral set			Dextral set		
		δ estimated value	δ true value	Difference	δ estimated value	δ true value	Difference
0°	20%	−55°	−57°	2°	55°	53°	2°
	30%	−55°	−58°	3°	55°	51°	4°
	40%	−55°	−59°	4°	55°	52°	3°
	50%	−55°	−53°	2°	55°	56°	1°
10°	20%	−53°	−49°	4°	58°	54°	4°
	30%	−54°	−54°	1°	57°	55°	1°
	40%	−54°	−58°	4°	56°	57°	1°
	50%	−55°	−60°	5°	56°	56°	1°
20°	20%	−49°	−48°	0°	62°	70°	8°
	30%	−50°	−52°	2°	60°	69°	9°
	40%	−52°	−54°	2°	58°	65°	7°
	50%	−53°	−58°	5°	57°	64°	7°
30°	20%	−40°	−39°	1°	71°	76°	5°
	30%	−46°	−44°	2°	65°	70°	6°
	40%	−48°	−50°	3°	63°	67°	4°
	50%	−51°	−51°	1°	60°	62°	3°
40°	20%	−38°	−36°	2°	73°	78°	6°
	30%	−40°	−41°	1°	70°	75°	5°
	40%	−42°	−48°	6°	68°	70°	2°
	50%	−45°	−48°	4°	66°	72°	7°

If we assume that σ_1 is parallel to Z, then for the model with layers oriented parallel to X ($\varphi_0 = 0^\circ$) the value predicted by equation (3) is equivalent to the angle ζ between shear fractures and σ_1. A critical point arising from this observation is the large predicted value of ζ and its reconciliation with theoretical criteria. Large values of shear fracture angles ($\zeta > 45^\circ$) are mechanically unfavourable (Vermeer, 1990) and are not expected to occur because such angles imply macroscopic strain hardening of the material (e.g. Kaus, 2010). However, Issen and Rudnicki (2000) and Mair et al. (2000) described the formation of shear bands in granular materials with angles $\zeta > 45^\circ$ due to cataclastic grain size reduction and pressure-driven processes. Although our models experienced compaction, some of the physical processes described by these authors (i.e. grain size reduction, dissolution and cementation) do not take place in our experiments. On the other hand, several field and experimental observations in deformed ductile materials reported high dihedral angles between conjugate fracture sets, with a σ_1 parallel to the obtuse bisector between conjugate fracture sets (e.g. Cobbold et al., 1971; Platt and Vissers, 1980; White et al., 1980; Behrmann, 1987; Harris and Cobbold, 1984; Hanmer et al., 1996; Kidan and Cosgrove, 1996). For example, Gomez-Rivas et al. (2007) used an analytical method to describe the nucleation of small-scale faults in quartzites located within a Variscan shear zone. They calculated that these faults nucleated at an angle ζ considerably higher than 45° with respect to the σ_1 inferred from field structural analysis. High angles between fractures and σ_1 are normally interpreted as a consequence of large bulk deformation and fracture rotation towards the extension direction (e.g. Gomez-Rivas et al., 2007; Scholz, 2007) or pre-existing frictionally weak surfaces (e.g. Collettinni et al., 2009; Fagereng et al., 2010). This is coherent with numerical simulation results by Mancktelow (2002), who used power-law viscous rheologies to simulate stretching faults. The large dihedral angles between conjugate sets in our experiments can be explained considering: (a) the low propagation velocities of the existing fractures as a consequence of ductile deformation at their tips, which favours their simultaneous rotation while they propagate, and (b) the influence of heterogeneities in the material that affect the orientation of the developed brittle fractures and shear bands.

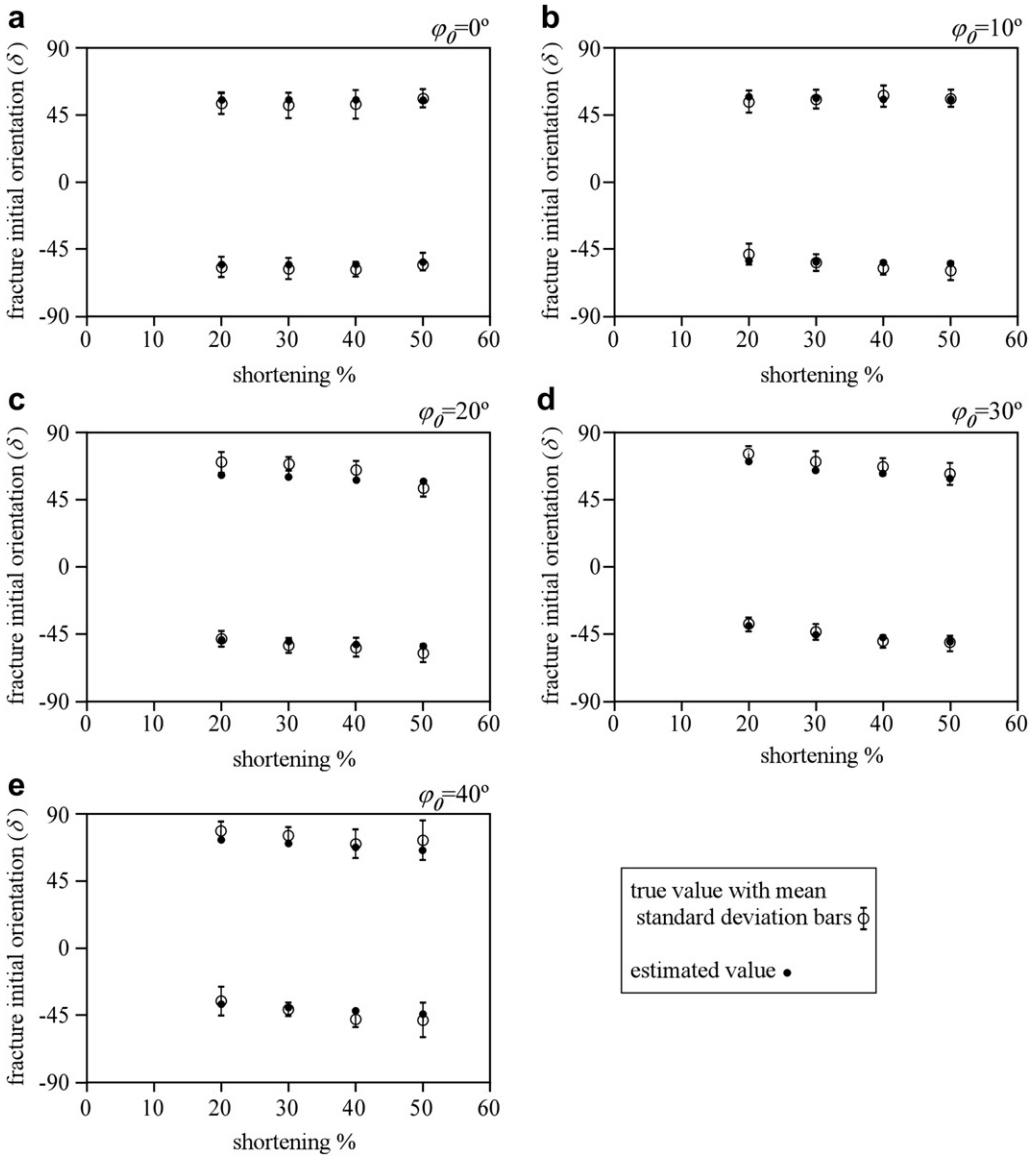

Fig. 15. Comparison of measured (open dots) and estimated (closed dots) values of the initial angles at which shear fractures nucleate. The good fit to both groups of data show that equation (3) can be used to explain the nucleation angle of new shear fractures in all the experiments. The vertical bars indicate the mean standard deviation of each data set.

4.2. On the influence of anisotropy on the evolution of existing shear fractures with progressive deformation

Fractures and shear bands are generally assumed to rotate as passive material lines towards the extension direction with increasing ductile deformation. However, Fig. 14b shows that shear fractures rotate at an angular velocity ω considerably slower than the one expected for a passive material line. Their rotation velocity is similar to the one measured for layers. For models with the anisotropy oriented parallel to the maximum extension axis X ($\varphi = 0^\circ$), both sets of fractures rotate towards the extension direction: the dextral set rotates sinistrally while the sinistral one rotates dextrally (Fig. 14a). However, in the models with oblique anisotropy ($\varphi > 0^\circ$) the dextral set of fractures does not rotate according to the imposed boundary conditions (Fig. 14b). In this case, the sinistral set rotates dextrally towards the X-direction, while the dextral set also rotates dextrally. In such cases, both fracture sets rotate together in a dextral sense towards the external extensional axis X. The obtuse bisector between both sets is approximately parallel to the layer normal at all deformation stages for all the experiments (i.e. for all the possible orientations of anisotropy (φ)).

Since part of the vorticity is being accommodated by layer rotation (dextral sense), and the bulk vorticity needs to be balanced according to the coaxial boundary conditions, the system tends to develop a different amount of dextral and sinistral shear fractures. This can be observed from the smaller fracture index (Fig. 13) and shorter length of the dextral set of shear fractures compared to the sinistral ones in $\varphi > 0^\circ$ cases. Dextral fractures are subjected to a higher normal stress and, therefore, they cannot easily propagate and slip. According to Scholz (2007), slip along pre-existing fractures is locked up at angles close to 60° with σ_1. Contrary to the dextral case, sinistral shear fractures are subjected to lower normal stress and higher shear stress, and consequently they have a more favourable orientation for slip and propagation.

Our observations are in accordance with those of Misra et al. (2009), which present experiments using a non-cohesive sand-talc mixture. These authors found that two sets of shear fractures

are formed when the material is isotropic, and that increasing the degree of anisotropy results in the growth of only one set of shear fractures. Their theoretical analysis, based on an elastic-anisotropic media, revealed that for strongly anisotropic materials only one fracture set is developed and it tends to be formed at a low angle with respect to the external σ_1. However, their solution is only valid for instantaneous deformation. The results of our plasticine experiments, which take into account the time-dependent evolution of the system, also indicate the predominance of one fracture set in anisotropic systems with layering or foliation oriented oblique to the stress/strain axis, despite the differences in the mechanical behaviour between our experimental materials and that of Misra et al. (2009).

4.3. On the influence of anisotropy on the stress field orientation

As summarised in Fig. 12 and Table 5, models with layering oblique to X ($\varphi_0 \neq 0^\circ$) show a marked asymmetry of fracture density, length and orientation between the two conjugate sets of shear fractures, despite the coaxial boundary conditions. This indicates a possible deviation between the local deformation field and the stress field imposed by the deformation rig. According to the Coloumb criterion, conjugate sets of shear fractures should develop symmetrically with respect to the principal stresses. Therefore, the principal compressive and tensile stress axes should be located at the bisectors of the dihedral regions between conjugate fracture sets (e.g. Ramsay and Lisle, 2000). If we apply this premise to our fracture data, we would conclude that in our experiments the inferred σ_1 would be located in the obtuse bisector between conjugate fracture sets (see Fig. 12) and would be oriented approximately perpendicular to layering. For the $\varphi_0 = 0^\circ$ model the inferred σ_1 stress is indeed approximately parallel to the compressive stress applied by the deformation apparatus (Fig. 16). However, the inferred σ_1 for the $\varphi_0 \neq 0^\circ$ models does not coincide with the applied boundary conditions. A substantial deviation between the inferred and the applied stress fields is observed with increasing layer obliquity (Fig. 16). For example, for the $\varphi_0 = 40^\circ$ experiment, the angle between the inferred and applied stresses was 24° when the first fractures nucleated (at approx. 20% shortening; Fig. 16). This angle decreased with progressive deformation, and the inferred stress field rotated towards the orientation of the imposed stress field. At the same time, the asymmetry between the two fracture sets was considerably reduced. However, differences in fracture density, orientation and length between both sets still remained at the end of the experiment. The sinistral set in our oblique models is more intensively developed in terms of fracture density and length than the dextral one because it is oriented at a lower angle to the σ_1 applied by the boundary conditions (Figs. 12 and 13). Therefore, sinistral fractures are subjected to a lower normal stress than dextral ones. Several field studies also reported local deviations of the orientation of faults with respect to the regional stress conditions for layered and anisotropic rocks (e.g. Bradshaw and Zoback, 1988; Peacock and Sanderson, 1992). Two general observations can be extracted from our modelling results and the literature: (a) the stress and strain rate fields are not always parallel in anisotropic materials and (b) their angular difference depends on the degree of anisotropy (e.g. Cosgrove, 1976; Weijermars, 1992; Treagus, 1998; Kocher and Mancktelow, 2006; Toimil and Griera, 2007).

Our observations indicate that anisotropy not only produces a deviation of the local deformation field with respect to the imposed boundary conditions, but also induces a change in the orientation of the shear fracture sets. For the case of plane-strain coaxial deformation two important points arise from our experiments: (1) the obtuse bisector between conjugate sets is not always coincident with σ_1 and (2) the asymmetry between conjugate fracture sets is related to the degree and orientation of anisotropy

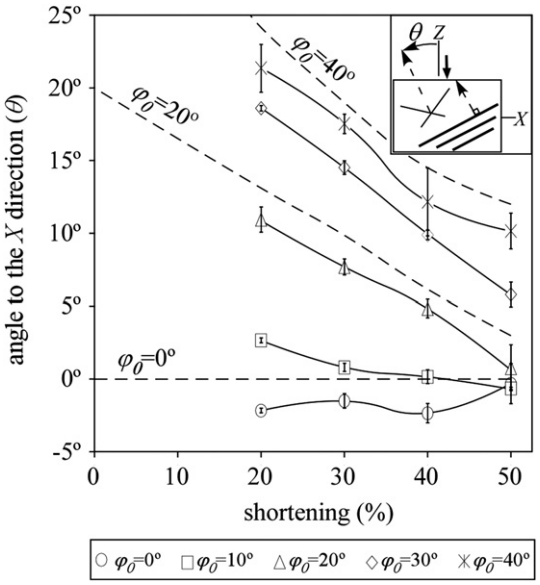

Fig. 16. Evolution with increasing deformation of the angle θ between the obtuse bisector of the two sets of shear fractures and the maximum shortening axis Z. Dashed lines show the orientation of anisotropy planes with the maximum extension axis X. The vertical bars indicate the mean standard deviation of each data set.

with regard to the stress and strain axes. Both considerations imply that caution must be taken in the field when stress field orientations are calculated from conjugate fracture sets if the rocks are anisotropic.

Similar observations have also been made by other authors from field studies in rocks deformed under brittle-viscous conditions. For example, Mancktelow and Pennacchioni (2005) and Pennacchioni and Mancktelow (2007) reported large angles between conjugate shear zone sets in foliated granitoids from the Eastern Alps. They concluded that these shear zones resulted from the reactivation of pre-existing structures such as dykes, quartz veins and joints in a coaxial deformation regime with a horizontal σ_1. In their study, the sinistral and dextral sets of shear zones form low and high angles with respect to σ_1, respectively (see Figs. 15 and 16 of Pennacchioni and Mancktelow, 2007). Moreover, σ_1 is also perpendicular to the bulk foliation and opening features mainly occur in the sinistral domain. These observations and interpretations are coherent with our observations and show that, despite of the limitations of the experiments, our results can be used to improve the current knowledge on the influence of anisotropy on the orientation and evolution of shear fracture networks.

5. Conclusions

This contribution presents an experimental study of the influence of anisotropy on the nucleation and evolution of shear fracture networks in an elastoviscous material that is subjected to ductile and brittle deformation. Several anisotropic plasticine multilayers were deformed under coaxial boundary conditions while varying the initial orientation of anisotropy with regard to the deformation axes. We aim to simulate situations of deformation at low effective confining pressures, such as expected for middle- to lower crust rocks with high fluid pressures or local extension conditions. The analysis of the resulting fracture networks led to the following main conclusions:

1. The presence of a strong anisotropy has a significant influence on the angle at which shear fractures nucleate. In models with

layering oriented parallel to the extension axis two symmetrical sets of shear fractures develop, while these arrays are asymmetric for models with oblique anisotropy. Fracture nucleation angles in these experiments can be predicted with a simple equation (eq. (3)).

2. The dihedral angles between conjugate fracture sets are always higher than 100° and the obtuse bisectors between these sets are perpendicular to layers at all deformation stages. The calculated stress field inferred from fracture data in models with anisotropy oblique to the deformation axes differs from the boundary conditions applied by the experimental device. Differences on fracture density, orientation and length between shear fracture sets or are potential indicators of the deviation of σ_1 with respect to the obtuse bisector between conjugate sets. This deviation is controlled by the degree of anisotropy and the amount of deformation.This indicates that caution must be taken when stress field orientations are calculated from fracture orientation data in the field if the rocks are anisotropic.
3. The average angle ζ between the obtuse bisector and fracture sets is always higher than 45°. As the obtuse bisector is parallel to the applied σ_1 in the experiment with layers oriented parallel to the extension axis ($\varphi_0 = 0°$), we can conclude that the angles between fractures and σ_1 do not fit with the classical failure criteria (i.e. lower than 45°) and differ from the observations of other authors in brittle anisotropic rocks. This can be due to the lack of layer slipping, the strong ductile behaviour of the material and the low propagation rates of shear fractures in our models.
4. Anisotropy also plays a crucial role in the rotation of fractures. In models with oblique anisotropy both sets of fractures rotate jointly with layering towards the extension direction *X*. Hence, the dextral array rotates in an opposite sense than the one expected from the boundary conditions.

Acknowledgements

This work was financed through the PhD grant BES-2003-0755 to EGR and research project CGL2004-03657, both funded by the Spanish Ministry of Education and Science. We thank J. Carreras and E. Druguet for discussions on various aspects related to this work, to P.D. Bons and M.W. Jessell for many valuable suggestions and to L.M. Castaño for her assistance during some of the experiments. We gratefully acknowledge N. Timms and A. Fagereng, whose constructive reviews greatly improved the manuscript, together with the editorial guidance of T.G. Blenkinsop. We would also like to thank G. Zulauf, F. Marques and D. Koehn for their comments to a previous version of the manuscript.

References

Al-Harthi, A.A., 1998. Effect of planar structures on the anisotropy of Ranyah sandstone, Saudi Arabia. Engineering Geology 50, 49–57.
Arslan, A., Passchier, C.W., Koehn, D., 2008. Foliation boudinage. Journal of Structural Geology 30, 291–309.
Attewell, P.B., Sandford, M.R., 1974. Intrinsic shear strength of a brittle, anisotropic rock-I: experimental and mechanical interpretation. International Journal of Rock Mechanics and Mining Sciences & Geomechanics Abstracts 11, 423–430.
Atkinson, B.K., 1987. Introduction to fracture mechanics and its geophysical applications. In: Atkinson, B.K. (Ed.), Fracture Mechanics of Rock. Academic Press, San Diego (CA), pp. 1–26.
Behrmann, J.H., 1987. A precautionary note on shear bands as kinematic indicators. In: Cobbold, P.R., Gapais, D., Means, W.D., Treagus, S.H. (Eds.), Shear Criteria in Rocks. Journal of Structural Geology 9. Pergamon, Oxford-New York, pp. 659–666.
Bons, P.D., Jessell, M.W., 1995. Strain analysis in deformation experiments with pattern matching or a stereoscope. Journal of Structural Geology 17, 917–921.
Bons, P.D., Druguet, E., Hamann, I., Carreras, J., Passchier, C.W., 2004. Apparent boudinage in dykes. Journal of Structural Geology 26, 625–636.
Bons, P.D., Druguet, E., Castaño, L.-M., Elburg, M.A., 2008. Finding what is now not there anymore: recognizing missing fluid and magma volumes. Geology 36, 851–854.
Bons, P.D., Becker, J.K., Elburg, M.A., Urtson, K., 2009. Granite formation: stepwise accumulation of melt or connected networks? Earth and Environmental Science Transactions of the Royal Society of Edinburgh 100, 105–115.
Bradshaw, G.A., Zoback, M.D., 1988. Listric normal faulting, stress refraction, and the state of stress in the Gulf Coastal Basin. Geology 16, 271–274.
Chenevert, M.E., Gatlin, C., 1965. Mechanical anisotropies of laminated sedimentary rocks. Journal of the Society of Petroleum Engineers 5, 67–77.
Cobbold, P.R., Cosgrove, J.W., Summers, J.M., 1971. Development of internal structures in deformed anisotropic rocks. Tectonophysics 12, 23–53.
Collettinni, C., Niejmeijer, A., Viti, C., Marone, C., 2009. Fault zone fabrics and fault weakness. Nature 462, 907–910.
Cosgrove, J.W., 1976. The formation of crenulation cleavage. Journal of the Geological Society of London 132, 155–178.
Davidson, C., Schmid, S.M., Hollister, L.S., 1994. Role of melt during deformation in the deep crust. Terra Nova 6, 133–142.
Donath, F.A., 1961. Experimental study of shear failure in anisotropic rocks. Geological Society of America Bulletin 72, 985–990.
Druguet, E., Carreras, J., 2006. Analogue modelling of syntectonic leucosomes in migmatitic schists. Journal of Structural Geology 28, 1734–1747.
Fagereng, A., Remitti, F., Sibson, R.H., 2010. Shear veins observed within anisotropic fabric at high angles to the maximum compressive stress. Nature Geoscience 3, 482–485.
FitzGerald, J.D.F., Boland, J.N., McLaren, A.C., Ord, A., Hobbs, B.E., 1991. Microstructures in water-weakened single crystals of quartz. Journal of Geophysical Research 96, 2139–2155.
Fossen, H., 2010. Structural Geology. Cambridge University Press, 480 pp.
Fusseis, F., Regenauer-Lieb, K., Liu, J., Hough, R.M., De Carlo, F., 2009. Creep cavitation can establish a dynamic granular fluid pump in ductile shear zones. Nature 459, 974–977.
Gomez-Rivas, E., Bons, P.D., Griera, A., Carreras, J., Druguet, E., Evans, L., 2007. Strain and vorticity analysis using small-scale faults and associated drag folds. Journal of Structural Geology 29, 1882–1899.
Gomez-Rivas, E., Griera, A., 2009. Influence of mechanical anisotropy on shear fracture development. Trabajos de Geología 29, 305–311.
Gomez-Rivas, E., Griera, A., 2011. Strain rate influence on fracture development in experimental ductile multilayers. Tectonophysics 502, 345–357.
Hanmer, S., Corrigan, D., Ganas, A., 1996. Orientation of nucleating faults in anisotropic media: insights from three-dimensional deformation experiments. Tectonophysics 267, 275–290.
Harris, L.B., Cobbold, P.R., 1984. Development of conjugate shear bands during bulk simple shearing. Journal of Structural Geology 7, 37–44.
Hoek, E., 1968. Brittle fracture of rock. In: Stagg, K.G., Zienkiewicz, O.C. (Eds.), Rock Mechanics in Engineering Practice. Wiley, pp. 99–124.
Hudson, J.A., Harrison, J.P., 1997. Engineering Rock Mechanics: An Introduction to the Principles. Pergamon, New York.
Ishii, K., 1992. Partitioning of non-coaxiality in deforming layered rock masses. Tectonophysics 210, 33–43.
Issen, K.A., Rudnicki, J.W., 2000. Conditions for compaction bands in porous rock. Journal of Geophysical Research-Solid Earth 105 (B9), 21529–21536.
Jaeger, J.C., Cook, N.G.W., 1979. Fundamentals of Rock Mechanics. Chapman and Hall, New York.
Jiang, D., 1994. Vorticity determination, distribution, partitioning and the heterogeneity and non-steadiness of natural deformations. Journal of Structural Geology 16, 121–130.
Kaus, B.J.P., 2010. Factors that control the angle of shear bands in geodynamic numerical models of brittle deformation. Tectonophysics 484, 36–47.
Kidan, T.W., Cosgrove, J.W., 1996. The deformation of multilayers by layer normal compression: an experimental investigation. Journal of Structural Geology 18, 461–474.
Kocher, T., Mancktelow, N.S., 2006. Flanking structure development in anisotropic viscous rock. Journal of Structural Geology 28, 1139–1145.
Lister, G.S., Williams, P.F., 1983. The partitioning of deformation in flowing rock masses. Tectonophysics 92, 1–33.
Mair, K., Main, I., Elphick, S., 2000. Sequential growth of deformation bands in the laboratory. Journal of Structural Geology 22, 25–42.
Mancktelow, N.S., 1988. The rheology of paraffin wax and its usefulness as an analogue for rocks. Bulletin of Geological Institutions of the University of Uppsala 14, 181–193.
Mancktelow, N.S., 1999. Finite-element modelling of single-layer folding in elasto-viscous materials: the effect of initial perturbation geometry. Journal of Structural Geology 21, 161–177.
Mancktelow, N.S., 2002. Finite-element modelling of shear zone development in viscoelastic materials and its implications for localisation of partial melting. Journal of Structural Geology 24, 1045–1053.
Mancktelow, N.S., Pennacchioni, G., 2005. The control of precursor brittle fracture and fluid-rock interaction on the development of single and paired ductile shear zones. Journal of Structural Geology 27, 645–661.
Mandl, G., 2000. Faulting in Brittle Rocks. Springer-Verlag, Berlin–Heidelberg–New York.
Marchildon, N., Brown, M., 2003. Spatial distribution of melt-bearing structures in anatectic rocks from Southern Brittany: implications for melt transfer at grain- to orogen-scale. Tectonophysics 364, 215–235.

McClay, K.R., 1976. Rheology of plasticine. Tectonophysics 33, T7–T15.
McGill, G.E., Raney, J.A., 1970. Experimental study of faulting in an anisotropic, inhomogeneous dolomitic limestone. Geological Society of America Bulletin 81, 2949–2958.
McLamore, R., Gray, K.E., 1967. The mechanical behavior of anisotropic sedimentary rocks. Journal of Engineering for Industry (Transactions of the American Society of Mechanical Engineering) 89, 62–73.
Misra, S., Mandal, N., Chakraborty, C., 2009. Formation of Riedel shear fractures in granular materials: findings from analogue shear experiments and theoretical analyses. Tectonophysics 471, 253–259.
Peacock, D.C.P., Sanderson, D.J., 1992. Effects of layering and anisotropy on fault geometry. Journal of the Geological Society of London 149, 793–802.
Pennacchioni, G., Mancktelow, N.S., 2007. Nucleation and initial growth of a shear zone network within compositionally and structurally heterogeneous granitoids under amphibolite facies conditions. Journal of Structural Geology 29, 1757–1780.
Pfiffner, O.A., Ramsay, J.G., 1982. Constraints on geological strain rates: arguments from finite strain states naturally deformed rocks. Journal of Geophysical Research 87, 311–321.
Platt, J.P., Vissers, R.L.M., 1980. Extensional structures in anisotropic rocks. Journal of Structural Geology 2, 397–410.
Poliakov, A.B., Herrmann, H.J., Podladchikov, Y.Y., Roux, S., 1994. Fractal plastic shear bands. Fractals 2, 567–581.
Pollard, D.D., Fletcher, R.C., 2005. Fundamentals of Structural Geology. Cambridge University Press.
Price, N.J., Cosgrove, J.W., 1990. Analysis of Geological Structures. Cambridge University Press.
Ramsay, J.G., Lisle, R.J., 2000. The Techniques of Modern Structural Geology. In: Applications of Continuum Mechanics in Structural Geology, vol. 3. Academic Press, London.
Ranalli, G., 1995. Rheology of the Earth. Chapman & Hall, London.
Reches, Z., Lockner, D.A., 1994. Nucleation and growth of faults in brittle rocks. Journal of Geophysical. Research 99 (B9), 18,159–18,173.
Rybacki, E., Wirth, R., Dresen, G., 2008. High-strain creep of feldspar rocks: implications for cavitation and ductile failure in the lower crust. Geophysical Research Letters 35, L04304.
Scholz, C.H., 2002. The Mechanics of Earthquakes and Faulting. Cambridge University Press.
Scholz, C.H., 2007. Fault mechanics. In: Schubert, G. (Ed.), Treatise on Geophysics. Elsevier, Amsterdam, pp. 441–483.
Schöpfer, M.P.J., Zulauf, G., 2002. Strain-dependent rheology and the memory of plasticine. Tectonophysics 354, 85–99.
Schöpfer, P.J., Childs, C., Walsh, J.J., 2006. Localisation of normal faults in multilayer sequences. Journal of Structural Geology 28, 816–833.
Stunitz, H., FitzGerald, J.D., Tullis, J., 2003. Dislocation generation, slip systems, and dynamic recrystallization in experimentally deformed plagioclase single crystals. Tectonophysics 372, 215–233.
Tikoff, B., Fossen, H., 1995. The limitations of three-dimensional kinematic vorticity analysis. Journal of Structural Geology 17, 1771–1784.
Toimil, N.C., Griera, A., 2007. Influence of viscosity contrast and anisotropy on strain accommodation in competent layers. Journal of Structural Geology 29, 787–801.
Treagus, S.H., 1997. Deformation partitioning in folds: implications for fold geometry and cleavage patterns. In: Sengupta, S. (Ed.), Evolution of Geological Structures in Micro- to Macro-Scales. Chapman and Hall, London, pp. 341–372.
Treagus, S.H., 1998. Strain refraction in layered systems. Journal of Structural Geology 10, 517–527.
Treagus, S.H., Sokoutis, D., 1992. Laboratory modelling of strain variation across rheological boundaries. Journal of Structural Geology 14, 405–424.
Twiss, R.J., Moores, E.M., 1992. Structural Geology. W.H. Freeman and Company, New York.
Vardoulakis, I., 1980. Shear band inclination and shear modulus of sand in biaxial tests. International Journal for Numerical and Analytical Methods in Geomechanics 4, 103–119.
Vermeer, P.A., 1990. The orientation of shear bands in biaxial tests. Géotechnique 40, 223–236.
Vernooij, M.G.C., Kunze, K., den Brok, B., 2006. 'Brittle' shear zones in experimentally deformed quartz single crystals. Journal of Structural Geology 28, 1292–1306.
Weijermars, R., 1997. Principles of Rock Mechanics. Alboran Science Publishing, Amsterdam.
Weijermars, R., 1992. Progressive deformation in anisotropic rocks. Journal of Structural Geology 14, 723–742.
Weijermars, R., Schmeling, H., 1986. Scaling of Newtonian and non-Newtonian fluid dynamics without inertia for quantitative modelling of rock flow due to gravity (including the concept of rheological similarity). Physics of the Earth and Planetary Interiors 43, 316–330.
Welch, M.J., Davies, R.K., Knipe, R.J., Tueckmantel, C., 2009. A dynamic model for fault nucleation and propagation in a mechanically layered section. Tectonophysics 474, 473–492.
White, S., Burrows, S., Carreras, J., Shaw, N., Humphreys, F., 1980. On mylonites in ductile shear zones. Journal of Structural Geology 2, 175–187.
Zhang, Y., Hobbs, B.E., Ord, A., Mühlhaus, H.B., 1996. Computer simulation of single-layer buckling. Journal of Structural Geology 18, 643–655.
Zulauf, J., Zulauf, G., 2004. Rheology of plasticine used as rock analogue: the impact of temperature, composition and strain. Journal of Structural Geology 26, 725–737.